

RESEARCH/REVIEW ARTICLE

Near-surface eddy dynamics in the Southern Ocean

Marilisa Trani^{1,2}, Pierpaolo Falco¹ & Enrico Zambianchi¹¹ Department of Environmental Science, Parthenope University of Naples, Centro Direzionale, Isola C4, IT-80143 Naples, Italy² Doctoral School in Polar Sciences, University of Siena, Via del Laterano 8, IT-53100 Siena, Italy**Keywords**

Antarctic Circumpolar Current; eddy fluxes; Global Drifter Program data; Lagrangian oceanography; Helmholtz decomposition.

Correspondence

Marilisa Trani, Department of Environmental Science, Parthenope University of Naples, Centro Direzionale, Isola C4, IT-80143 Naples, Italy.

E-mail: marilisa.trani@uniparthenope.it

Abstract

The Antarctic Circumpolar Current (ACC) is a crucial component of the global ocean conveyor belt, acting as a zonal link among the major ocean basins but, to some extent, limiting meridional exchange and tending to isolate the ocean south of it from momentum and heat income. In this work we investigate one of the most important mechanisms contributing to the poleward transfer of properties in the Southern Ocean, that is the eddy component of the dynamics. For this particular purpose, observations obtained from near-surface drifters have been used: they represent a very useful data set to analyse the eddy field because of their ability to catch a large number of scales of motion while providing a quasi-synoptic coverage of the investigated area. Estimates of the eddy heat and momentum fluxes are carried out using data taken from the Global Drifter Program databank; they refer to Surface Velocity Program drifter trajectories collected in the area south of 35°S between 1995 and 2006. Eddy kinetic energies, variance ellipses, momentum and heat fluxes have been calculated using the pseudo-Eulerian method, showing patterns in good agreement with those present in the literature based on observational and model data, although there are some quantitative differences. The eddy fluxes have been separated into their rotational and divergent portions, the latter being responsible for the meridional transports. The associated zonal and depth-exponentially integrated meridional heat transport exhibits values spanning over a range between -0.4 PW and -1.1 PW in the ACC region, consistent with previous estimates.

The Southern Ocean has a distinctive and complex dynamics, mainly due to its circumpolar extent and to the absence of land barriers in the latitude band of Drake Passage. It is characterized by two main circulations which are intimately linked: a mainly zonal wind-driven circulation, the Antarctic Circumpolar Current (ACC; see reviews by Nowlin & Klinck 1986; Rintoul et al. 2001; Olbers et al. 2004) and a meridional overturning circulation (Doos & Webb 1994; Speer et al. 2000; Olbers & Visbeck 2005).

Being a large and strong eastward-flowing current, the ACC tends to isolate the warm subtropical waters from the cold polar waters, acting primarily as a barrier to the

inter-basin exchange of heat and other properties between the Southern Ocean and the rest of the global ocean.

On the other hand, the Ekman pumping due to the strong and persistent wind regime induces an upwelling of deep water south of the latitude of maximum wind intensity, where there is a divergence of the Ekman transport and a downwelling north of it, creating the so-called Deacon cell, which needs to be closed at depth by a poleward flowing branch. This closure is most likely provided by the eddy field, originated in the meandering, highly turbulent ACC; the eddy field transfers the energy input by the wind through the water column down to the

bottom, where it is eventually dissipated by the form drag; it also represents the mechanism which transports momentum, heat and other properties across the ACC (Munk & Palmen 1951; Johnson & Bryden 1989; Marshall & Radko 2003).

Therefore, as a result of the connection provided by eddies, a three-dimensional ocean circulation develops, embedded in the global thermohaline circulation, contributing to the central role played by the Southern Ocean in regulating the Earth's climate, through the formation, transformation and redistribution of water masses throughout the other three major oceans.

For many years eddy momentum and heat fluxes have represented poorly observed quantities, mainly because of the sparseness of available hydrographic data; recently, the interest in quantifying more accurately these fluxes, especially in the Southern Ocean, has considerably grown, thanks also to the improvement and diffusion of measuring techniques such as satellite altimetry and drifting buoys (Keffer & Holloway 1988; Stammer 1998; Phillips & Rintoul 2000; Jayne & Marotzke 2002; Gille 2003). This allows not only to improve eddy parameterizations in ACC dynamics models, but also for a recent re-evaluation of the role of lateral eddy-induced mixing in determining the vertical structure of the ACC (LaCasce & Isachsen 2010).

As shown by an assessment of hydrographic and altimetric measurements of eddy heat fluxes in the ocean, carried out by Wunsch (1999), and also by the results obtained by Jayne & Marotzke (2002), who calculated these fluxes using a global high-resolution ocean general circulation model, high values of eddy heat fluxes can be observed in the ACC as well as in the western boundary currents, while they are generally weaker in the interior of ocean gyres. This suggests that the mesoscale eddy field plays a crucial role in the time-mean ocean heat transport and stresses its importance in climate processes.

According to Gordon & Owens (1987), who adopted an indirect approach, a heat flux of -0.3 PW crossing the Polar Front is necessary to balance the heat lost to the atmosphere at higher latitudes. Direct estimates of near-surface eddy heat fluxes require repeated measurements of both temperature and velocity: for the Southern Ocean a very first value of -0.5 PW was obtained by Bryden (1979), who extrapolated it for the entire ACC from estimates drawn on the basis of hydrographic data in the Drake Passage, but such an extrapolation cannot be considered reliable, given the high spatial inhomogeneity of these fluxes (Stammer 1998; Jayne & Marotzke 2002; Gille 2003).

Further estimates from hydrographic data led to a value of -0.45 PW (DeSzoek & Levine 1981), whereas values spanning between -0.7 PW (Keffer & Holloway 1988) and -0.05 PW (Stammer 1998) were derived from altimetric measurements; a recent work by Gille (2003) on the basis of autonomous Lagrangian circulation explorer (ALACE) float data indicates a range between -0.3 ± 0.1 and -0.6 ± 0.3 PW.

The main difficulty with using hydrographic data lies in the sparseness of the observations, which prevents from having the required resolution to measure the entire variability of the eddy field. On the other hand, estimates based on altimetry rely on the assumption that eddy heat fluxes are proportional to large-scale temperature gradients (Gille 2003), and they therefore cannot detect equatorward directed fluxes. Gille's (2003) approach on the basis of ALACE float data, which provide quasi-Lagrangian measurements of temperature and velocity at 900 m of depth, possibly represents one of the best methods to capture eddy variability with satisfactory data coverage.

In this article we analyse the variability of the Southern Ocean circulation using Lagrangian data from near-surface drifters, i.e., using Gille's (2003) methodology but applying it to the sea surface, with a higher spatial and temporal resolution, and using data relative to a longer period. Dynamical considerations allow us to retrieve the component of the eddy field which is actually responsible for the meridional heat transport, as done by Jayne & Marotzke (2002). As discussed by Marshall & Shutts (1981), the eddy field can be considered as composed of two different dynamical components: a rotational component, which does not contribute to the globally integrated poleward transport of heat by the ocean, since it transports as much energy into any given region as it does out of the region itself; and a divergent component, which actually affects the local heat budget, and therefore is dynamically active. Therefore, Helmholtz decomposition was carried out to separate eddy fluxes into their rotational and divergent portions.

Utilized data and methods are presented in the second section; in the third section the variability of the velocity field is described while in the fourth we illustrate the main distribution of the eddy heat fluxes and report on the results of transport estimation; in the fifth section we discuss and summarize our findings.

Data and methods

In this work we have analysed Surface Velocity Program (SVP) drifter data taken from the Global Drifter Program (GDP; Lumpkin & Pazos 2007) databank, deployed in the

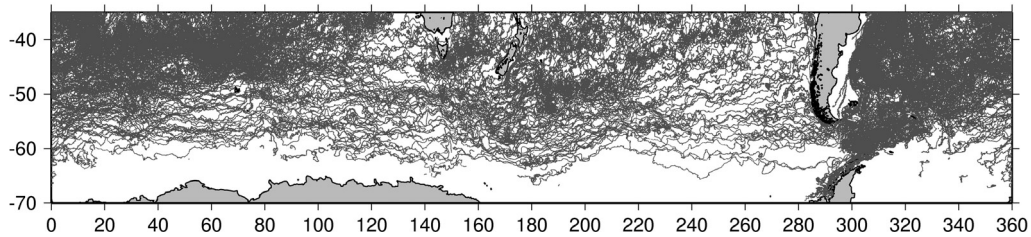


Fig. 1 World Ocean Circulation Experiment Surface Velocity Program drifters trajectories from 1995 to 2006 in the selected area from 70°S to 35°S around the globe.

Southern Ocean between 1995 and 2006, consisting of locations and sea surface temperatures (SSTs).

SVP drifters are tracked by the Argos system onboard the US National Oceanic and Atmospheric Administration (NOAA) polar-orbiting satellites and consist of two parts: a surface float and a subsurface drogue. The surface float contains batteries, a satellite transmitter, a thermistor for sub-skin SST and sometimes other instruments measuring barometric pressure, wind speed and direction, salinity or ocean colour. The immersed drogue is centred at 15 m depth, and it is of the holey-sock type; this design reduces the wind slip maximizing the near-surface current drag (Lumpkin & Pazos 2007). Drifters that have lost their drogue were not considered in our analysis.

Although the temperature sensor is located 30 cm below the surface, while the velocities are relative to the drogue mid-depth, the two values can be related to each other since temperature can be considered homogeneous in the first 10–20 m during all seasons as observed in previous studies (De Boyer Montegut et al. 2004; Dong et al. 2008; Sallée et al. 2008).

GDP data are processed and distributed by NOAA's Atlantic Oceanographic and Meteorological Laboratory, where velocities are calculated on the basis of 6-hourly interpolated positions (Hansen & Poulain 1996).

Figure 1 shows the drifter trajectories in the selected area (70°S–35°S around the globe); while in Fig. 2 we report the amount of available data per year and per season (summer, from October to March; winter, from April to September). The yearly distribution is characterized by a sharp discontinuity in the total number of observations occurred in 2001, when it started to increase significantly until 2004, to then decrease to levels anyway higher than those attained in the first six years of observations (1995–2000). The seasonal data coverage is approximately constant for the whole observational period with the only exception on the 2005, when winter observations drastically decreased.

The temporal data distribution was evaluated in different parts of the domain and a map of seasonal

bias was built (shown in Fig. 3). Each drifter position's date was identified with a complex number, with unit amplitude and phase set by the year-day (0° for 1 January, 180° for 2 July and so on), and the average was computed for each bin (Lumpkin 2003). The resulting amplitude represents a measure of the homogeneity of the sampling through the seasons in that bin. According to Lumpkin (2003) significantly biased mean is obtained past the threshold value of 0.3: here 43% of the bins are below this value, the most biased region being a thin zonal band near 60°S (Fig. 3). Some separate calculations for winter and summer data are included to evaluate differences in the results. Since the distribution of the eddy heat fluxes shows a non-Gaussian, but rather closer to a bi-exponential, distribution (as evaluated following Chinn & Gille (2007)), our results based on averages were compared with computations based on medians, which did not show noticeable differences.

Pseudo-Eulerian analysis

Even though in principle this is a very broad definition, which includes all the dynamics developing at scales smaller than the mean field, that is, mesoscale, sub-mesoscale etc., down to the dissipation scales, as an operational hypothesis we assume that the eddy field is represented by the residual fluctuation v' with respect to

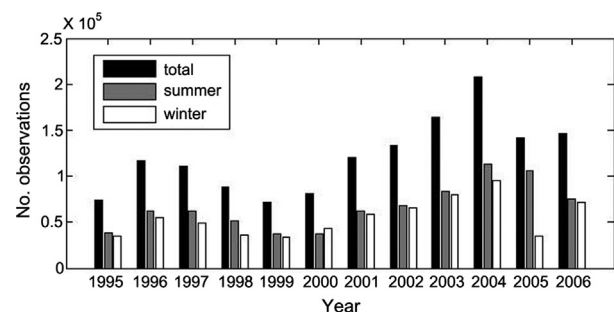


Fig. 2 Yearly and seasonal overall data distributions on the domain. Summer includes months from October to March and winter from April to September.

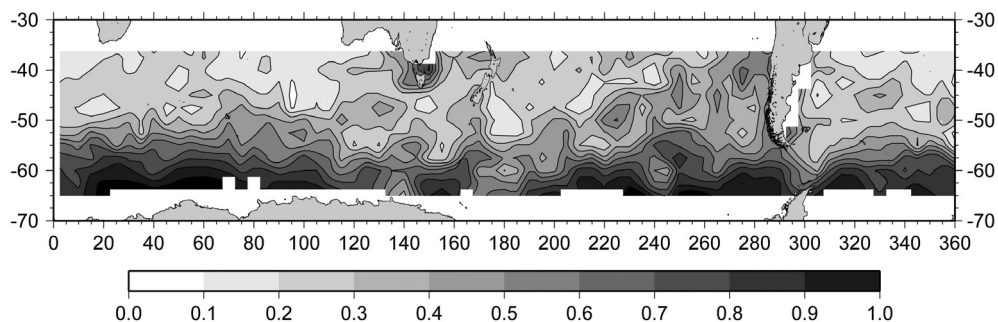


Fig. 3 Amplitude of the seasonal observational bias. An amplitude near zero indicates nearly homogeneous sampling, while amplitudes near unity show where one season is sampled exclusively.

the mean flow \bar{v} (e.g., Falco & Zambianchi 2011); therefore, first of all an accurate estimate of the mean flow has to be drawn. Following an Eulerian-based method, the so-called binning technique (Poulain & Niiler 1989; Davis 1991a, b), drifter velocities can be grouped in spatial sub-regions (bins) that are assumed to have quasi-homogeneous dynamical properties, and then averaged to obtain a distribution of the mean circulation. A crucial aspect of the binning method is represented by setting the optimal bin dimension. The bin should be large enough to contain as many drifter observations as necessary to guarantee robust statistics; on the other hand, it should be small enough to give sufficient spatial resolution, allowing for a detailed representation of the mean field and of its dynamical features (e.g., jets, meanders, convergence and divergence areas). A compromise then is necessary to balance the two opposite needs and this may not be totally straightforward.

To mention a few recent approaches, Lumpkin & Garaffo (2005) determined first the direction of the axis of maximum velocity variance of the current field and then oriented the bins according to this axis. This method was recently applied by Sallée et al. (2008) to GDP drifter data gathered in the Southern Ocean during the decade 1995–2005 to study the Lagrangian eddy statistics and the diffusivity distribution in this area. They used 5° longitude by 1° latitude wide bins.

Falco & Zambianchi (2011) applied the method proposed by Bauer et al. (1998) to determine the large scale, time-independent component of the ACC current field. They determined the mean flow fitting the data with bicubic splines that are continuous functions, thus allowing for very high spatial resolution, particularly efficient in fitting data that are irregularly distributed and with high levels of superimposed noise (Inoue 1986). The mean field resulting from the spline interpolation was compared with that obtained by simple binning over 5° longitude by 2.5° latitude bins and, in terms of the overall pattern, the two results were in very good agreement.

Considering the general aim of this work to analyse larger scale structures, in order to emphasize the spatial variability among different areas of the Southern Ocean as a first step, a high spatial resolution of the current is not a priority, whereas it is important to obtain robust statistics evaluated in each bin, we therefore decided to apply the straight binning method in Cartesian coordinates. On the basis of the results described in Falco & Zambianchi (2011), 5° longitude by 2.5° latitude wide bins were chosen, corresponding, at these latitudes, approximately to square areas with sides of 250 km. Such dimensions guarantee a statistically relevant data density in most of the bins, furthermore, providing a comprehensive view of the ACC mean field and eddy field at the upper mesoscale lengths.

As consequence of the bin dimension, the number of independent observations range from 10 to 200 for the most part of the domain, considering a mean integral eddy time scale of two days (Rupolo 2007; Sallée et al. 2008). Bins with less than 100 velocity observations, which correspond to approximately six independent observations and are less statistically significant, were not considered in the subsequent calculations.

Patterns of the mean field and of the eddy kinetic energy (EKE) obtained with a smaller bin size, of 2° in longitude and 1° in latitude were evaluated as well, and, as expected, they present slightly finer structures, but are not qualitatively very different from those presented here. Nevertheless, higher values are found in the maxima due to the diminished data density per bin, which leads to a further sampling bias due to the increased spatial inhomogeneities. When using Lagrangian data, the spatial biases are more evident in regions of higher EKE since drifters preferentially sample zones of high EKE (Hofmann 1985; Garraffo et al. 2001).

In each bin, zonal and meridional deviations from the mean (u', v') have been calculated by subtracting the zonal and meridional components of $\bar{v}(\bar{u}, \bar{v})$ from all Lagrangian velocities in that bin ($u' = u - \bar{u}$; $v' = v - \bar{v}$).

From (u', v') we have computed in each bin the EKE and the variance ellipses (see Preisendorfer 1988). After computing the variance associated to the zonal and meridional velocity components in each bin and their covariance, the direction κ of the axis of principal variability is

$$\tan\theta = \frac{\sigma_{11} - \overline{u'^2}}{\overline{u'v'}}, \quad (1)$$

Where the variance along the major axis is given by

$$\sigma_{11} = \frac{1}{2}(\overline{u'^2} + \overline{v'^2} + \sqrt{(\overline{u'^2} - \overline{v'^2})^2 + 4(\overline{u'v'})^2}), \quad (2)$$

and along the minor axis by

$$\sigma_{22} = (\overline{u'^2} + \overline{v'^2}) - \sigma_{11}, \quad (3)$$

The elongation of the ellipse provides an estimate of the anisotropy of the field, and the direction of the major axis represents the principal direction of the residual velocity variability. Its magnitude depends on the covariance term $\overline{u'v'}$, so it can also provide information about the eddy momentum flux direction: ellipses with a major axis oriented toward the north-east (south-east) quadrant have a positive (negative) $\overline{u'v'}$, indicating a northward (southward) directed eddy momentum flux.

Eddy heat flux calculation

Near-surface eddy heat fluxes have been estimated using the classical expression $\rho_0 C_p \overline{v'T'}$, where ρ_0 is the mean seawater density taken to be 1025Kg/m^3 , C_p is the specific heat of water at constant pressure taken to be $4000 \text{J/(kg}^\circ\text{C)}$ and $\overline{v'T'}$ is the eddy heat flux vector field, whose zonal component $\overline{u'T'}$ is the covariance of the zonal component of the velocity and of the temperature and whose meridional component $\overline{v'T'}$ is the covariance of the meridional component of the velocity and of the temperature, where T' is the residual fluctuation of T in the bin. These estimates have also been performed separating winter and summer data.

To retrieve the divergent part of this flux which, as previously explained, is the fraction of the total eddy heat flux actually responsible of the transport of heat, we carried out Helmholtz decomposition.

Helmholtz decomposition

In the area of vector calculus, the Helmholtz's theorem states that a vector field \mathbf{V} may be written as the sum of a solenoidal and an irrotational part, which constitutes the so-called Helmholtz decomposition:

$$\mathbf{V} = \mathbf{V}_\psi + \mathbf{V}_\chi, \quad (4)$$

On a two-dimensional surface these components can be represented by a streamfunction ψ of the solenoidal component,

$$\mathbf{V}_\psi = \kappa \times \nabla\psi, \quad (5)$$

with κ being the unit vector normal to the surface and ∇ the horizontal gradient vector, and a potential function χ of the irrotational component:

$$\mathbf{V}_\chi = \nabla\chi, \quad (6)$$

In geophysical fluid dynamics this decomposition has been used first in atmospheric dynamics studies (Sangster 1960; Shukla & Saha 1974; Lau & Wallace 1979), and then was introduced in oceanography for the analysis of eddy vector fields, where the divergent part of the flux results to be of particular dynamical interest (Marshall & Shutts 1981; Watterson 2001; Jayne & Marotzke 2002).

The Helmholtz decomposition can be carried out by solving the Poisson equations obtained for the vertical component of the curl of \mathbf{V} in Eqn. 4; taking into account Eqn. 5, we get the following equation for ψ :

$$\nabla^2\psi = \zeta, \quad (7)$$

where ζ is the curl of \mathbf{V} , that is, the relative vorticity. Taking the divergence of \mathbf{V} in Eqn. 4, from Eqn. 6 we obtain the following equation for χ :

$$\nabla^2\chi = D, \quad (8)$$

where D is the divergence of \mathbf{V} .

According to Helmholtz's theorem, the decomposition is unique in an infinite domain, assuming that the fluxes decay rapidly enough as infinity is approached. In contrast, in a limited domain the Poisson equation is not solvable in a straightforward manner because the divergent and rotational fluxes cannot be observed individually, and without using additional constraints these fluxes and their boundary conditions cannot be determined uniquely (Fox-Kemper et al. 2003).

For this reason several different methods have been developed to specify boundary conditions: the classical ones are of the Dirichlet type and of the Neumann type. The Dirichlet type requires specifying the values of ψ and χ at the boundaries, whereas the Neumann type requires specifying their normal derivatives at the boundaries, for example, setting them as zero at the coasts, as was done by Jayne & Marotzke (2002). Some combinations of these two methods have also been attempted (e.g., Lynch 1989), with the help of iterative procedures to adjust the solution so as to get more accurate results, but these procedures often have the disadvantage to be both

numerically and computationally expensive (see Li et al. (2006) for an exhaustive review).

Different approaches to the decomposition problem have been proposed and tested by Griesel et al. (2009) and Smith (2008). Smith (2008) developed an algorithm based on the Fast Fourier Transform and tested it in a coastal environment obtaining satisfactory results, but to our knowledge this method was not tried in open ocean areas. Griesel et al. (2009) used two alternative methods: the first based on eddy length scales, trying to remove the rotational component of the total eddy fields by averaging over certain length scales; the second based on the physical considerations discussed by Marshall & Shutts (1981), according to which the rotational component can be approximated by its projection along temperature variance contours. However, they found that both these methods leave a residual that is not entirely divergent and still contains a large fraction of the rotational component. To perform the decomposition in the Southern Ocean, we have implemented a method which provides a unique solution without the necessity to impose boundary conditions. This is very advantageous when this kind of calculation is applied to a domain like the Southern Ocean, which has no continuous solid boundaries at its northern and southern sides; therefore, the zero condition at the coasts is not sufficient, and additional zonal boundary conditions are required where it confines with the other oceans. In general, the computation of the streamfunction and of the potential from the velocity field is an inverse and ill-posed problem in classical inverse problem theory that can be solved by Tikhonov regularization (Tikhonov & Arsenin 1977). This was previously done by Li et al. (2006), who provided a unique solution without the need to impose explicit boundary conditions for ψ and χ , computing them for an irregular domain near a coast.

In our work, Eqns. 7 and 8 have been discretized with the method of finite volumes (Varga 1965) on a staggered grid (Fig. 4), where ψ and χ have been set as all internal (crosses and encircled crosses) with respect to the points where the values of the vector field \mathbf{V} are given (dots). The integration of Eqns. 7 and 8 around the internal

points of the grid (crosses) leads to uncoupled discrete equations for ψ and χ . On the other hand, the integration of Eqns. 7 and 8 near the boundary points (encircled crosses) leads to coupled equations for ψ and χ . So the final discretized system to be solved is

$$\begin{cases} A\mathbf{q}_\psi + B\mathbf{q}_\chi = \mathbf{p}_\psi \\ B\mathbf{q}_\psi + A\mathbf{q}_\chi = \mathbf{p}_\chi \end{cases}, \quad (9)$$

where A and B are respectively the uncoupled and the coupled matrices of the coefficients; \mathbf{p}_ψ and \mathbf{p}_χ the vectors of the known terms, dependent respectively from ζ , v_x , v_y and D , v_x , v_y , at the dots in Fig. 4 (v_x and v_y are the components of the eddy heat vector field, i.e., \overline{uT} and \overline{vT}); \mathbf{q}_ψ and \mathbf{q}_χ are the vectors of the unknown ψ and χ at the crosses and encircled crosses in Fig. 4.

Then the system (10) can be reduced to:

$$M\mathbf{q} = \mathbf{p} \text{ with } M = \begin{bmatrix} A & B \\ B^T & A \end{bmatrix}, \quad (10)$$

The solution is found minimizing the norm $\|M\mathbf{q} - \mathbf{p}\|^2$ through the Tikhonov regularization.

The size of the matrix to be inverted can affect output values at the boundaries, as emerged from additional tests we carried out extending the domain to the north. There were no significant changes of the output values in the interior of the domain, while we noted some differences in their distribution at the boundaries. The same test cannot be done to the south of the domain because of the lack of data there.

Mean field and eddy variability

The mean velocity field (Fig. 5) shows a distribution quite similar, qualitatively, to the result of previous analyses carried out on the basis of First GARP Global Experiment (FGGE) drifter data (Patterson 1985; Piola et al. 1987). Quantitatively, our estimates result lower for two main reasons: first of all, FGGE data refer to a shorter period with respect to the data set used in this work; therefore, capturing a smaller portion of the signal, possibly stronger than the longer term average; in the second place, considering the design of the drifters used during

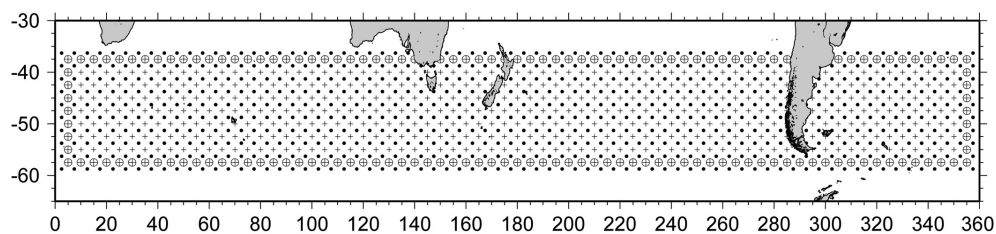


Fig. 4 Decomposition grid. Dots represents the values of the known vector field \mathbf{V} ; crosses and encircled crosses are the points in which ψ and χ have been calculated, the former with uncoupled discrete equations, the latter with coupled equations.

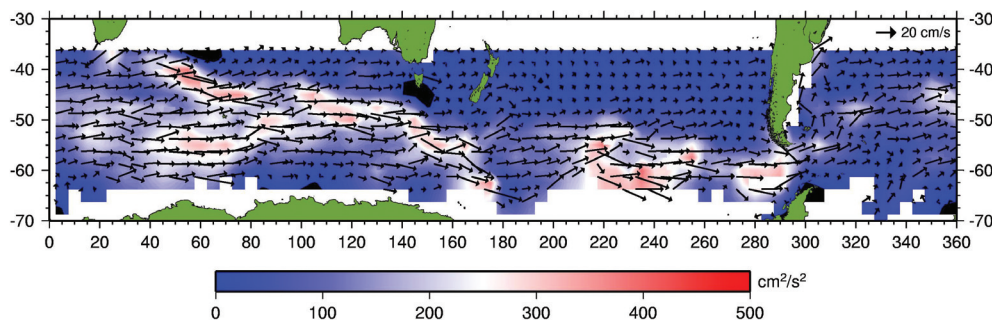


Fig. 5 Mean velocity field (black arrows) obtained from drifters data ensemble averaged on 5° longitude by 2.5° latitude bins. The underlying coloured pattern represents the mean kinetic energy field. Values in bins with less than 100 observations have been removed. For the main topographic features positions see Fig. 6.

the FGGE experiment, those data could contain a supplement of energy due to the wind (Piola et al. 1987; Niiler & Paduan 1995; see also the discussion in Falco & Zambianchi [2011]).

In Fig. 5 high values of the velocity can be seen in the Agulhas Retroflection south of Africa and in the ACC regions, while the lowest ones can be observed in the interior of the South Pacific Ocean sector with speeds smaller than 5–10 cm/s. This is the area of the Southern Ocean which presents the broadest transition between the Antarctic and the Subtropical waters, and with the weakest dynamics. These weak flows are due to the fact that the South Pacific Current, which follows the Subtropical Front, is much weaker than its counterparts in the Atlantic and Indian oceans (Stramma et al. 1995); in addition, a prominent low-salinity signal extending westward from Chile along 41°S due to the high precipitation and river runoff (Deacon 1937, 1977; Neshyba & Fonseca 1980; Orsi et al. 1995) contributes to lower property gradients.

South of Africa a broader band of velocities with values of 20–30 cm/s can be identified, while the flow appears to undergo a sort of channelling after passing Kerguelen Island, flowing eastward in a narrower band with large meanders, until reaching Drake Passage, after which it broadens again. This channel effect is induced by bottom topography which steers the current (Marshall 1995), as can be easily observed in Fig. 5, where higher velocities indicate a prevailing flow following the Southeast Indian Ridge and the Pacific–Antarctic Ridge, which narrows near the main fracture zones of the Australian Antarctic Discordance, in the Indian Ocean Sector at 120°E , and the Udintsev and Eltanin fracture zones, in the Pacific Sector at 220°E – 230°E .

The EKE distribution (Fig. 6) is also influenced by the bottom topography; maxima can be observed near the major topographic features crossed by the ACC (Campbell Plateau, Pacific–Antarctic Ridge, Drake Passage). The

strongest values of the EKE, between 2000 and 3000 cm^2/s^2 , are found in the regions of the Agulhas Retroflection and the Brazil–Malvinas Confluence, while, as previously noted, the interior of the South Pacific Sector exhibits the weakest flows, and also presents the weakest variability with the lowest observed values of EKE, less than 200 cm^2/s^2 . This pattern is very similar to results presented by Sallée et al. (2008), although their estimates are quantitatively higher, especially in the areas where the variability is particularly strong, that is, in the Agulhas Retroflection and the Brazil–Malvinas Confluence. This is likely due to the different binning technique they used, with bins of smaller size oriented toward the direction of maximum variability, leading to an estimation of the fluctuating part that is higher than that obtained here. As discussed above in section 2.1 our choice in terms of bin size was motivated by the need to attain a good statistical significance, even though possibly inducing a weak smoothing.

Our first step in the analysis of the eddy field consists in characterizing the variability of the velocity field through the variance ellipses (Fig. 7), which show the principal direction of variability providing an estimate of the anisotropy of the field. Higher anisotropy can be seen near the major topographic features and near the coasts and the tendency of ellipses is to align with them, as previously noticed by Morrow et al. (1994). In general, anisotropy can also be observed where there is a strongly meandering current; this is true also for the ACC where, even far from main topographic features, variance ellipses relative to meandering regions are more elongated than in other areas, with the major axes increasing up to 1000 cm^2/s^2 , while in the core of the South Indian, South Atlantic, and even more evidently in the South Pacific sector, it does not exceed 100 cm^2/s^2 .

The orientation of variance ellipses, as stated in section 2.1, depends mainly on the covariance term of the zonal and meridional velocity components, so the direction of

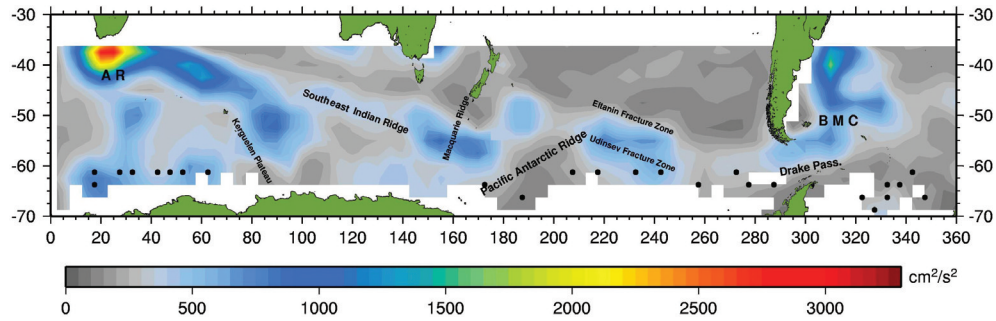


Fig. 6 Eddy kinetic energy with the main topographic features superimposed. Black circles point out bins with less than 100 observations; blanks south of 35°S are areas with only one independent observation or no data. The two major current systems of the Agulhas Retroflexion (AR) and the Brazil–Malvinas Confluence (BMC) are also indicated.

the principal ellipse axes corresponds to that of turbulent fluxes: an orientation towards the north-east (south-west) means a positive (negative) covariance with a corresponding northern (southern) transfer of momentum by the turbulent flow (Morrow et al. 1994). Eddy momentum fluxes can be simply represented by the covariance term if we consider the ACC as a purely zonal flow. Their pattern (Fig. 8) is very similar, although slightly higher absolute values, to that obtained by Morrow et al. (1994) from altimetric data averaged over a larger bin size of $5^\circ \times 5^\circ$ degrees, which can in part explain the small differences. However, a clear discrepancy shows up in the two regions along the Macquarie Ridge and the Pacific–Antarctic Ridge. We found there well-defined maxima in the negative fraction, which indicates southward eddy transport, that is, a subtraction of momentum from the mean field, whereas Morrow et al. (1994) found there a structure favorable to convergence of the eddy transport, with a resultant acceleration of the mean field. This discrepancy has been also noted by Hughes & Ash (2001), who found that some jets were decelerated by eddies and that the interaction with bottom topography was involved in this

mechanism. Nevertheless, they maintain that only the rotational part of the eddy field actually interacts with the mean field, so the comparison with the results obtained here is not straightforward.

Eddy heat fluxes and transport

As stated in the introduction, eddy heat fluxes are of fundamental importance in the Southern Ocean; in particular, their meridional component plays a crucial role in the Earth’s climate dynamics as it is responsible for the poleward heat transfer. The meridional eddy heat transport, represented by the meridional component of the covariance between velocity and temperature ($\overline{v'T'}$) is shown in Fig. 9a. The pattern is in good agreement with what Jayne & Marotzke (2002) obtained from data produced by a global high-resolution ocean general circulation model—the Parallel Ocean Climate Model (POCM)—though somewhat quantitatively higher in magnitude, and with a prevalence of negative values on positive ones. Maxima of southward eddy heat transport can be observed in the Agulhas Retroflexion, off the south-east coast of Australia, in the Brazil–

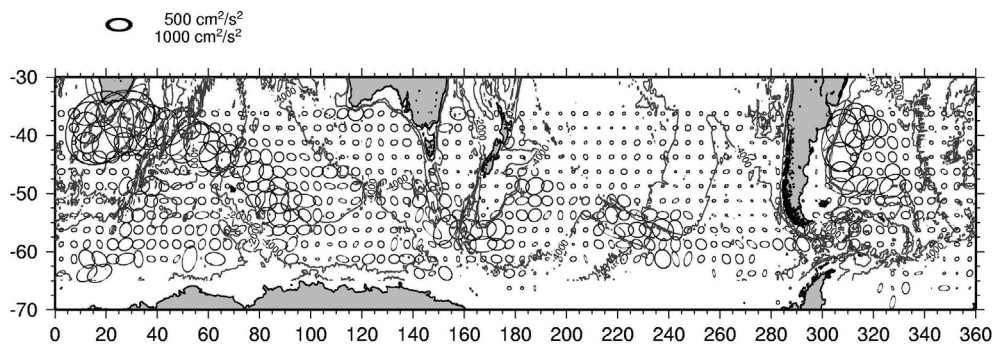


Fig. 7 Velocity variance ellipses. The scale ellipse has a semimajor axis of $1000 \text{ cm}^2 \text{ s}^{-2}$, a semiminor axis of $500 \text{ cm}^2 \text{ s}^{-2}$, and is rotated by 90° from north. The grey lines show the bottom topography.

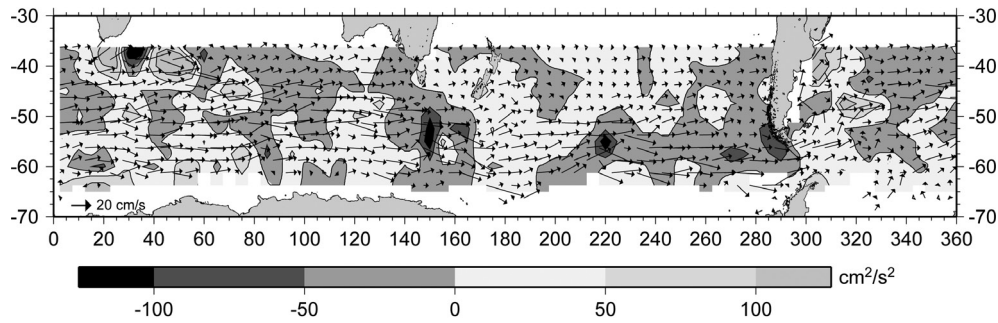


Fig. 8 Eddy momentum fluxes with the mean velocity field superimposed.

Malvinas Confluence and along an arch south of New Zealand. The quantitative discrepancy is most likely due to the fact that calculations with POCM underestimate mesoscale variability (Stammer et al. 1996), while estimates with drifters may show some bias in the regions of high EKE, as explained in the preceding section. Indeed, the highest discrepancies between the estimates obtained in this work and previous calculations are found in regions that also exhibit eddy kinetic energy maxima (see Fig. 6), that is, the Agulhas Retroflection, the Brazil–Malvinas Confluence and the ACC regions near the major topographic features (Kerguelen Plateau, Macquarie Ridge, Pacific–Antarctic Ridge and Drake Passage).

Seasonal meridional eddy heat fluxes, obtained separating winter and summer data in each bin with sufficient data coverage (not shown here), do not reveal significant qualitative differences, the relative patterns being quite similar. Differences between summer and winter $\overline{v'T'}$ values (Fig. 9b) point out overall slightly higher fluxes intensities during summer, although being statistically significant only south of Africa, off the west coast of New Zealand and near the Atlantic coast of South America. Furthermore, significantly higher values during winter in the Indian sector, downstream of the Kerguelen Plateau, are worth noticing. This result contrast in part with that of Sallée et al. (2006) who computed eddy heat fluxes by

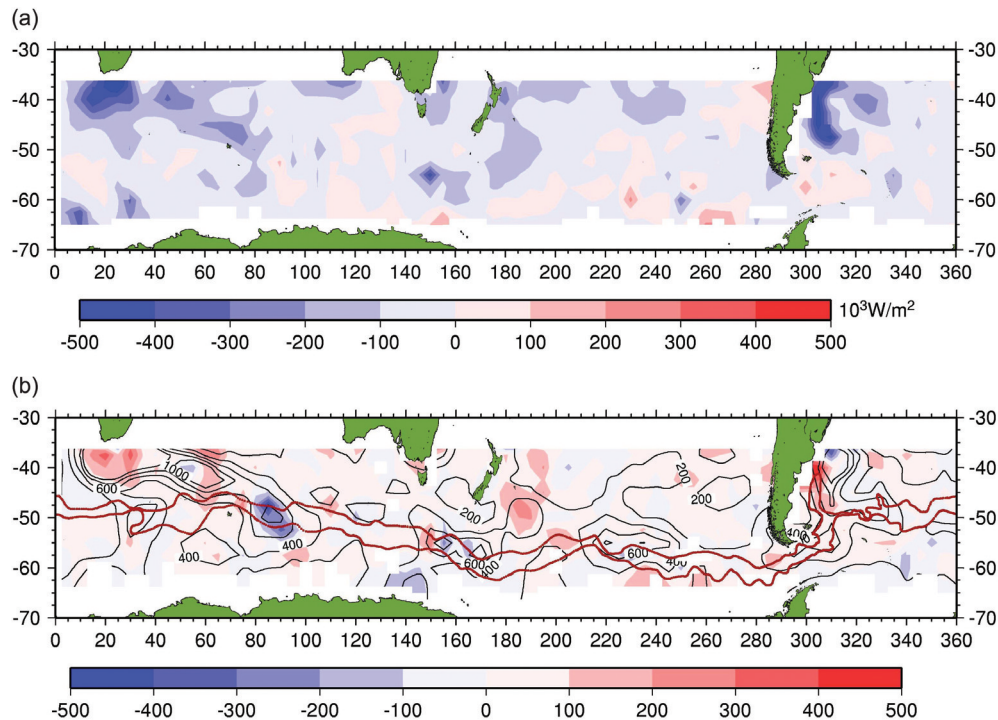


Fig. 9 (a) Meridional component of the eddy heat fluxes ($\overline{v'T'}$), obtained by all data in each bin; (b) differences between summer and winter meridional eddy heat fluxes, with superimposed the winter eddy kinetic energy field (thin black lines with annotated values in cm^2/s^2). Red lines show the position of the Subantarctic Front (SAF) and Polar Front (PF) from Orsi et al. 1995. Bins not statistically significant are left blank.

a parameterization using a diffusivity coefficient obtained by drifter data. They found the highest values of eddy heat fluxes upstream of the plateau and north of the Kerguelen Island, where ACC fronts are closer to each other, for this imply a sharp meridional temperature gradient. Indeed, our summer estimates match this pattern, while winter ones exhibit an eastward displacement of the maximum of poleward eddy heat fluxes, in a region downstream of the Kerguelen plateau. In Fig. 9b, the SAF and PF have been superimposed, together with the EKE field obtained by winter data. As can be seen, higher values of eddy heat fluxes are near the Kerguelen Island, where the two fronts are closer, while higher values in winter to the east coincide with an EKE winter maximum. This region has almost the same high meridional temperature gradient in both seasons, but the EKE summer maximum is further south, where meridional temperature gradients are much weaker (not shown here). The same winter and summer patterns differences can be observed also in the ACC region south of Australia, though at less extent.

Next, we estimated the rotational and divergent components of the eddy heat fluxes using the Helmholtz decomposition technique described earlier.

The distributions of the meridional components respectively of the rotational and of the divergent eddy heat transport are shown in Figs. 10 and 11, respectively. As we pointed out earlier, the rotational component does not contribute to the globally integrated poleward heat transport, as it carries as much energy into any given region as it does out of that same region, while the divergent component does affect the local heat budget, and therefore is dynamically active (Marshall & Shutts 1981). Therefore, as expected, the rotational component, exhibiting overall values higher than the divergent component shows an almost even distribution of positive and negative values; in contrast, negative values prevail in the divergent component pattern indicating a net poleward transport.

The distribution of the divergent component shows similarities as well as differences from the distribution obtained by Stammer (1998) and by Jayne & Marotzke (2002). Figure 11 shows that, from a qualitative point of view, the eddy heat transport is predominantly southward, with maxima in three areas: the Agulhas Retroflexion, the Brazil–Malvinas Confluence and south of New Zealand. The overall values are higher than previous estimates, though they are lower than those obtained simply considering the covariance term $\overline{v'T'}$. The main difference between our results and the estimates reported in the literature, and also from the distribution of $\overline{v'T'}$ (see Fig. 7) lies in the fact that it does not follow the ACC path, but appears more linked to the topography, with negative values upstream and positive values downstream of Kerguelen Plateau, Macquarie Ridge, Pacific–Antarctic Ridge and Drake Passage. In particular, the above positive values were not observed in previous works, but it is not clear whether they can be an artefact of the decomposition method used, for the output value distribution at the boundaries depends on the size of the domain over which the method is applied, as explained earlier.

The magnitude of the zonally and vertically integrated eddy heat transport is of crucial importance for the global heat budget of the Southern Ocean because eddies are the only mechanism through which heat can be transferred across the ACC balancing the heat loss at high latitudes. The first estimate of this quantity using Lagrangian data was carried out by Gille (2003) with ALACE floats providing temperatures and velocities at a depth of 900 m averaged over 9–25 day intervals.

Comparing her results with current meter data, Gille (2003) found that floats tended to underestimate the northward eddy heat transport, probably because of the unavoidable smoothing in time, so the resulting values were rescaled. Assuming a cross-ACC heat flux varying exponentially through the water column with an e -folding depth of 1000 m, Gille found a total meridional eddy heat flux ranging between -0.3 ± 0.1 and $-0.6 \pm$

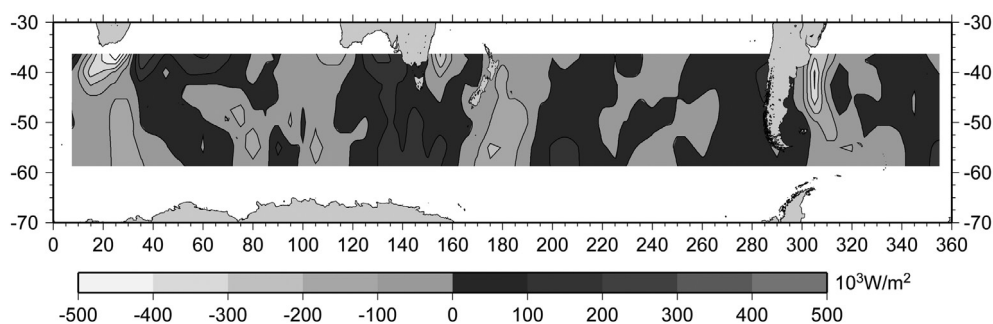


Fig. 10 Meridional component of the rotational eddy heat transport.

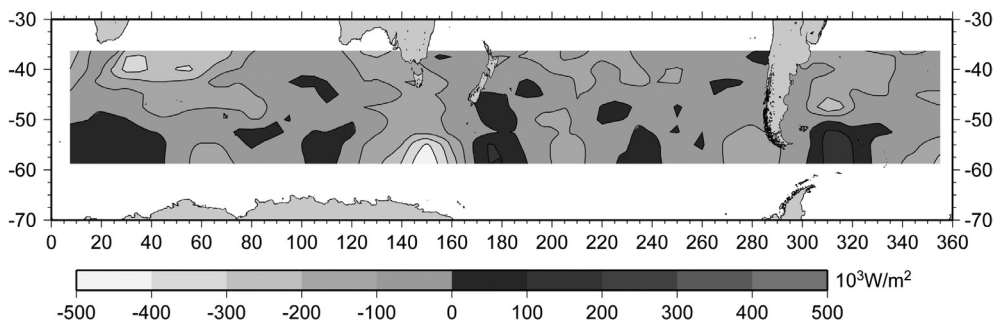


Fig. 11 Meridional component of the divergent eddy heat transport.

0.3 PW in the ACC core, where the ACC core was identified on the basis of a certain dynamic height range. In this work we have obtained estimates of zonally and vertically integrated eddy heat transport also assuming an exponential variation with an e -folding depth of 1000 m (Fig. 12). If we consider the ACC core as centred approximately between 45°S and 60°S, our estimates of meridional eddy heat transport are between -0.37 PW and -1.1 PW, in good agreement with Gille’s estimations in the direction across the mean flow; our estimate of -0.4 PW at 53 °S also agrees with DeSzoeke & Levine (1981), who determined a cross-ACC transport of -0.45 PW on the basis of hydrographic measurements. Generally speaking, the distribution shown in Fig. 12 is similar to other examples found in the literature (Keffer & Holloway 1988; Jayne & Marotzke 2002), but values are somewhat higher at lower latitudes due to the high energetic areas of the Agulhas Retroflection and the Brazil–Malvinas Confluence, which most likely account for the main part of the resulting zonal integral.

Summary and conclusions

In this work we used GDP surface drifter data collected between 1995 and 2006 to evaluate eddy momentum and heat fluxes in the Southern Ocean, focusing on the

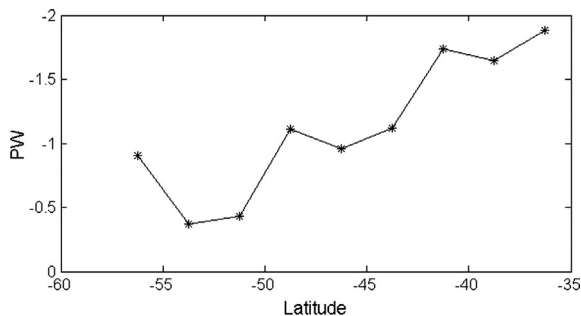


Fig. 12 Zonally and vertically integrated meridional component of the eddy heat transport.

meridional transport of heat across the ACC. To this end, we applied a pseudo-Eulerian technique (Davis 1991a,b), in which the mean field is estimated by averaging the data in geographical bins of 5° × 2.5°, and then subtracted from the data to obtain the fluctuating part.

The use of the binning technique causes a bias in the calculation of the mean field, and consequently of the eddy component, because drifters tend to converge toward the more energetic regions. This bias can be significantly reduced by keeping a good data density within the bins to have a more homogeneous spatial distribution and to ensure statistical reliability in the final estimates.

As expected, the mean velocity field is directed eastward and has a predominant zonal character, meanwhile showing some departures from the main linear course linked to the bottom topography, in particular, the ACC meanders and channels along the main bottom ridges and fracture zones (Gille 1997). The highest velocities, up to 20–30 cm/s, are found in the Agulhas Retroflection south of Africa and in the ACC, while the South Pacific sector interior exhibits the lowest values of less than 5–10 cm/s. The relation to the topography is also evident in the eddy field: the EKE exhibits maxima where the ACC encounters major topographic features along its path, with values up to 1000 cm²/s², and variance ellipses also present the highest anisotropy there, together with a tendency to align with the bottom topography. The highest values of EKE, up to 2000–3000 cm²/s², and a strong anisotropy with respect to the topography are observed in the Agulhas Retroflection and at the Brazil–Malvinas Confluence. The weakest and more isotropic eddy field can be seen in the interior of the South Pacific sector, with values of EKE lower than 200 cm²/s².

Eddy–mean field interactions have been evaluated analysing the eddy momentum flux distributions, that at a first approximation can be obtained from the covariance between the zonal and meridional component of the velocity $\overline{u'v'}$, considering the ACC as a purely zonal flow. Our pattern reveals strong similitude with that

obtained in previous works using altimetric data (Morrow et al. 1994; Hughes & Ash 2001). Like in Morrow et al. (1994), eddies mostly increase the ACC velocity, but, more noticeably, they work by reducing the speed of the mean current in two areas near the Macquarie Ridge and on the Pacific–Antarctic Ridge, as noted by Hughes & Ash (2001). However, Hughes and Ash (2001) considered only the fraction of the eddy field that actually interacts with the main flow (the rotational component). They retrieved this component by subtracting the EKE gradients from the total eddy momentum flux and interpreting the residual as an eddy vorticity flux. Since drifter have the tendency to converge toward the highly energetic frontal zones (Hofmann 1985), such a calculation may also help correct the bias in the velocity estimations in regions with high EKE. This issue will be the subject of a future work.

Eddy heat fluxes were computed to evaluate the meridional heat transport across the ACC, which is an important component in the thermodynamic balance of the Southern Ocean. This calculation was carried out first representing the meridional eddy heat fluxes as the covariance between the meridional component of the velocity and the temperature $\overline{v'T'}$. This exhibits a pattern similar to that by obtained by Jayne & Marotzke (2002) although with higher values: this is true for negative values, which are predominant in the distribution, but also for the maxima of the distribution, observed in the areas of the Agulhas Retroflection, off the south-east coast of Australia, the Brazil–Malvinas Confluence and along an arch south of New Zealand. On the other hand, the model used by Jayne & Marotzke (2002) underestimates the mesoscale variability while calculations with drifter data may present a small bias in regions with high EKE.

A separation of winter and summer data has been carried out to evaluate the possible influence of the seasonality in eddy heat fluxes calculations. Distributions obtained show similar patterns, with higher values during summer south of Africa, off the west coast of New Zealand and near the Atlantic coast of south America, except for a significantly higher value during winter in the Indian Ocean Sector, downstream of the Kerguelen Plateau. This is due to the fact that this area exhibits a maximum of EKE in winter. Since the Indian Ocean Sector is known to be an important region of winter Subantarctic Mode Water formation (Sallée et al. 2006), this result can be relevant in calculation of the rate of formation of these water masses, where eddy heat fluxes are generally regarded as not significant (Karstensen & Quadfasel 2002).

Then, the divergent component of the eddy heat flux has been estimated to consider the only fraction which is actually responsible of the meridional transport, as underlined by Marshall & Shutts (1981). The decomposition algorithm implemented here takes advantage of the mathematical technique of Tikhonov's regularization to solve the inverse problem, avoiding the difficulty of imposing boundary conditions. Although this approach does not prevent uncertain results at the boundaries, it does provide reliable values in the interior of the domain.

Rotational components of the fluxes exhibit higher values than the divergent ones, and a more even distribution between negative and positive values. It is worth noticing that the pattern of the divergent component is markedly different from previous estimates as its distribution appears strongly linked with the bottom topography rather than following the ACC path, with a marked transition from negative to positive values upstream and downstream the major topographic features, with a maximum across the Macquarie Ridge. A further explication of the observed discrepancies could be attributed to the use of zonal–meridional projection instead of across/along stream coordinates, which are more often considered in previous works regarding the Southern Ocean (e.g., Gille 2003; Sallée et al. 2008; Griesel et al. 2009).

Our estimates of the zonal and vertical integral of the meridional divergent eddy heat fluxes span a range between -0.37 PW and -1.1 PW, consistent with previous estimates by Gille (2003), although she did projection relative to the mean flow. The value at 53°S of -0.4 PW lies inside the previous range obtained from altimetric data by Keffer & Holloway (1988) and Stammer (1998), -0.7 PW and -0.05 PW respectively, and is very close to -0.45 PW evaluated by DeSzoek & Levine (1981) on the basis of hydrographic data.

The consistency of the integrated values of meridional eddy heat transports with previous estimates confirms the reliability of the method used to perform Helmholtz decomposition, despite some discrepancies which are in part due to the space/time inhomogeneity of Lagrangian data. Results obtained here, however, suggest a more important role of topography to the heat transport in the Southern Ocean, especially near the Macquarie Ridge and the Pacific–Antarctic Ridge, with respect to previous analysis based on altimetric and model data. We expect that a larger number of drifter observations, allowing to increase the resolution and the effectiveness of the decomposition technique, would yield more accurate and robust geographical patterns of the eddy heat transport. Further improvements of our decomposition

technique can also help to better evaluate the spatial distributions of eddy heat fluxes and to point out areas where most of the eddy heat transport occurs.

Acknowledgements

The authors warmly thank Giuseppe Buffoni for the fundamental support given to resolve the Helmholtz decomposition and Arnold L. Gordon for useful comments on an earlier version of this work. This article greatly benefited from the insightful input of an anonymous reviewer. This work was partly funded by the Italian National Programme for Antarctic Research. SVP drifter data have been kindly provided by NOAA's Atlantic Oceanographic and Meteorological Laboratory in Miami.

References

- Bauer S., Swenson M.S., Griffa A., Mariano A.J. & Owens K. 1998. Eddy—mean flow decomposition and eddy-diffusivity estimates in the tropical Pacific Ocean. 1. Methodology. *Journal of Geophysical Research—Oceans* 103, 30855–30871.
- Bryden H.L. 1979. Poleward heat flux and conversion of available potential energy in Drake Passage. *Journal of Marine Research* 37, 1–22.
- Chinn B.S. & Gille S.T. 2007. Estimating eddy heat flux from float data in the North Atlantic: the impact of temporal sampling interval. *Journal of Atmospheric and Oceanic Technology* 24, 923–934.
- Davis R.E. 1991a. Observing the general circulation with floats. *Deep-Sea Research Part I* 38, S531–S571.
- Davis R.E. 1991b. Lagrangian ocean studies. *Annual Review of Fluid Mechanics* 23, 43–64.
- Deacon G.E.R. 1937. The hydrology of the Southern Ocean. *Discovery Reports* 15, 3–122.
- Deacon G.E.R. 1977. Comments on a counterclockwise circulation in the Pacific Subantarctic sector of the Southern Ocean suggested by McGinnis. *Deep-Sea Research Part I* 24, 927–930.
- DeSzoek R.A. & Levine M.D. 1981. The advective flux of heat by mean geostrophic motions in the Southern Ocean. *Deep-Sea Research Part I* 28, 1057–1085.
- De Boyer Montégut C., Madec G., Fischer A., Lazar A & Iudicone D. 2004. Mixed layer depth over the global ocean: an examination of profile data and a profile-based climatology. *Journal of Geophysical Research—Oceans* 109, C12003, doi: 10.1029/2004JC002378.
- Dong S., Sprintall J., Gille S. & Talley L. 2008. Southern Ocean mixed-layer depth from Argo float profiles. *Journal of Geophysical Research—Oceans* 113, C06013, doi: 10.1029/2006JC004051.
- Döös K. & Webb D.J. 1994. The Deacon cell and other meridional cells of the Southern Ocean. *Journal of Physical Oceanography* 24, 429–442.
- Falco P. & Zambianchi E. 2011. Near-surface structure of the Antarctic Circumpolar Current derived from World Ocean Circulation Experiment drifter data. *Journal of Geophysical Research—Oceans* 116, C05003, doi: 10.1029/2010JC006349.
- Fox-Kemper B., Ferrari R. & Pedlosky J. 2003. On the indeterminacy of rotational and divergent eddy fluxes. *Journal of Physical Oceanography* 33, 478–483.
- Garraffo Z.D., Griffa A., Mariano A.J. & Chassignet E.P. 2001. Lagrangian data in a high resolution numerical simulation of the North Atlantic. II. On the pseudo-Eulerian averaging of Lagrangian data. *Journal of Marine Systems* 29, 177–200.
- Gille S. 1997. The Southern Ocean momentum balance: evidence for topographic effects from numerical model output and altimeter data. *Journal of Physical Oceanography* 27, 2219–2232.
- Gille S. 2003. Float observations of the Southern Ocean. Part II. Eddy fluxes. *Journal of Physical Oceanography* 33, 1182–1196.
- Gordon A.L. & Owens W.B. 1987. Polar oceans. *Review of Geophysics* 25, 227–233.
- Griesel A., Gille S.T., Sprintall J., McClean J.L. & Maltrud M.E. 2009. Assessing eddy heat flux and its parameterization: a wavenumber perspective from a 1/10° ocean simulation. *Ocean Modelling* 29, 248–260.
- Hansen D. & Poulain P.M. 1996. Quality control and interpolations of WOCE–TOGA drifter data. *Journal of Atmospheric and Oceanic Technology* 13, 900–909.
- Hofmann E.E. 1985. The large scale horizontal structure of the Antarctic Circumpolar Current from FGGE drifters. *Journal of Geophysical Research—Oceans* 90, 7087–7097.
- Hughes C.W. & Ash E.R. 2001. Eddy forcing of the mean flow in the Southern Ocean. *Journal of Geophysical Research—Oceans* 106, 2713–2722.
- Inoue H. 1986. A least-squares smoothing fitting for irregularly spaced data: finite-element approach using the cubic β -spline basis. *Geophysics* 51, 2051–2066.
- Jayne S.R. & Marotzke J. 2002. The oceanic eddy heat transport. *Journal of Physical Oceanography* 32, 3328–3345.
- Johnson G.C. & Bryden H.L. 1989. On the size of the Antarctic Circumpolar Current. *Deep-Sea Research Part I* 36, 39–53.
- Karstensen J. & Quadfasel D. 2002. Formation of Southern hemisphere thermocline waters: water mass conversion and subduction. *Journal of Physical Oceanography* 32, 3020–3038.
- Keffer T. & Holloway G. 1988. Estimating Southern Ocean eddy flux of heat and salt from satellite altimetry. *Nature* 332, 624–626.
- LaCasce J.H. & Isachsen P.E. 2010. The linear models of the ACC. *Progress in Oceanography* 84, 139–157.
- Lau N.C. & Wallace J.M. 1979. On the distribution of horizontal transports by transient eddies in the Northern Hemisphere wintertime circulation. *Journal of Atmospheric Science* 36, 1844–1861.

- Li Z.J., Chao Y. & McWilliams J.C. 2006. Computation of the streamfunction and velocity potential for limited and irregular domains. *Monthly Weather Review* 134, 3384–3394.
- Lumpkin R. 2003. Decomposition of surface drifter observations in the Atlantic Ocean. *Geophysical Research Letters* 30, article no. 1753, doi: 10.1029/2003GL017519.
- Lumpkin R. & Garaffo Z. 2005. Evaluating the decomposition of Tropical Atlantic Drifter observations. *Journal of Atmospheric and Oceanic Technology* 22, 1403–1415.
- Lumpkin R. & Pazos M. 2007. Measuring surface current with Surface Velocity Program drifters: the instrument, its data and some recent results. In A. Griffa et al. (eds.): *Lagrangian analysis and prediction of coastal and ocean dynamics (LAPCOD)*. Pp. 39–67. Cambridge? UK: Cambridge University Press.
- Lynch 1989. Partitioning the wind in a limited domain. *Monthly Weather Review* 117, 1492–1500.
- Marshall D. 1995. Topographic steering of the Antarctic Circumpolar Current. *Journal of Physical Oceanography* 25, 1636–1650.
- Marshall J. & Radko T. 2003. Residual mean solutions for the Antarctic Circumpolar Current and its associated overturning circulation. *Journal of Physical Oceanography* 33, 2341–2354.
- Marshall J. & Shutts G. 1981. A note on rotational and divergent eddy fluxes. *Journal of Physical Oceanography* 11, 1677–1680.
- Morrow R., Coleman R., Church J. & Chelton D. 1994. Surface eddy momentum flux and velocity variances in the Southern Ocean from Geosat altimetry. *Journal of Physical Oceanography* 24, 2050–2071.
- Munk W.H. & Palmen E. 1951. Note on dynamics of the Antarctic Circumpolar Current. *Tellus* 3, 53–55.
- Neshyba S. & Fonseca T.R. 1980. Evidence for counterflow to the west wind drift off South America. *Journal of Geophysical Research—Oceans* 85, 4888–4892.
- Niiler P.P. & Paduan J.D. 1995. Wind-driven motions in the northeast Pacific as measured by Lagrangian drifters. *Journal of Physical Oceanography* 25, 2819–2830.
- Nowlin E.W. & Klinck J.M. 1986. The physics of the Antarctic Circumpolar Current. *Review of Geophysics* 24, 489–491.
- Olbers D., Borowski D., Völker C. & Wölff J.O. 2004. The dynamical balance, transport and circulation of the Antarctic Circumpolar Current. *Antarctic Science* 16, 439–470.
- Olbers D. & Visbeck 2005. A model of the zonally averaged stratification and overturning in the Southern Ocean. *Journal of Physical Oceanography* 35, 1190–1205.
- Orsi A.H., Whitworth T.W. III & Nowlin W.D. Jr. 1995. On the meridional extent and fronts of the Antarctic Circumpolar Current. *Deep Sea Research Part I* 42, 641–673.
- Patterson S.L. 1985. Surface circulation and kinetic energy distributions in the Southern Hemisphere oceans from FGGE drifting buoys. *Journal of Physical Oceanography* 15, 865–884.
- Phillips H.E. & Rintoul S.R. 2000. Eddy variability and energetic from direct current measurements in the Antarctic Circumpolar Current south of Australia. *Journal of Physical Oceanography* 30, 3050–3076.
- Piola A.R., Figueroa A. & Bianchi A.A. 1987. Some aspects of the surface circulation south of 20° S revealed by first GARP Global Experiment drifters. *Journal of Geophysical Research—Oceans* 92, 5101–5114.
- Poulain P.M. & Niiler P.P. 1989. Statistical analysis of the surface circulation in the California Current System using satellite-tracked drifters. *Journal of Physical Oceanography* 19, 1588–1603.
- Preisendorfer R.W. 1988. *Principal component analysis in meteorology and oceanography*. Amsterdam: Elsevier.
- Rintoul S.R., Hughes C. & Olbers D. 2001. The Antarctic Circumpolar Current system. In G. Siedler et al. (eds.): *Ocean circulation and climate*. Pp. 271–302. New York: Academic Press.
- Rupolo V. 2007. A Lagrangian-based approach for determining trajectories taxonomy and turbulence regimes. *Journal of Physical Oceanography* 37, 1584–1609.
- Sallée J.B., Wienders N., Speer K. & Morrow R. 2006. Formation of Subantarctic mode water in the southeastern Indian Ocean. *Ocean Dynamics* 56, 525–542.
- Sallée J.B., Speer K., Morrow R. & Lumpkin R. 2008. An estimate of Lagrangian eddy statistics and diffusion in the mixed layer of the Southern Ocean. *Journal of Marine Research* 66, 441–463.
- Sangster W.E. 1960. A method of representing the horizontal pressure force without reduction of pressures to sea level. *Journal of Meteorology* 17, 166–176.
- Shukla J. & Saha K.R. 1974. Computation of non-divergent streamfunction and irrotational velocity potential from the observed winds. *Monthly Weather Review* 102, 419–425.
- Smith J.A. 2008. Vorticity and divergence of surface velocities near shore. *Journal of Physical Oceanography* 38, 1450–1468.
- Speer K., Rintoul S. & Sloyan B. 2000. The diabatic Deacon cell. *Journal of Physical Oceanography* 30, 3212–3222.
- Stammer D. 1998. On eddy characteristics, eddy transports, and mean flow properties. *Journal of Physical Oceanography* 28, 727–739.
- Stammer D., Tokmakian R., Semtner A.J. & Wunsch C. 1996. How well does a ¼ global circulation model simulate large-scale oceanic observations? *Journal of Geophysical Research—Oceans* 101, 25 779–25 811.
- Stramma L., Patterson R. & Tomczak M. 1995. The South Pacific Current. *Journal of Physical Oceanography* 25, 77–91.
- Tikhonov A.N. & Arsenin V. 1977. *Solution of ill-posed problems*. Washington, D.C.: Winston & Sons.
- Varga R.S. 1965. *Matrix iterative analysis*. Berlin: Springer.
- Watterson I.G. 2001. Decomposition of global ocean currents using a simple iterative method. *Journal of Atmospheric and Oceanic Technology* 18, 691–703.
- Wunsch C. 1999. Where do ocean eddy heat fluxes matter? *Journal of Geophysical Research—Oceans* 104, 13 235–13 249.